Machine Learning Thermo-Barometry: Application to Clinopyroxene-Bearing Magmas

Petrelli, Maurizio; Caricchi, Luca; Perugini, Diego

How to cite

PETRELLI, Maurizio, CARICCHI, Luca, PERUGINI, Diego. Machine Learning Thermo-Barometry: Application to Clinopyroxene-Bearing Magmas. In: Journal of Geophysical Research: Solid Earth, 2020. doi: 10.1029/2020JB020130

This publication URL: https://archive-ouverte.unige.ch/unige:140827
Publication DOI: 10.1029/2020JB020130

Petrelli Maurizio (Orcid ID: 0000-0001-6956-4742)
Caricchi Luca (Orcid ID: 0000-0001-9051-2621)
Perugini Diego (Orcid ID: 0000-0002-2888-6128)

Machine Learning Thermo-Barometry: Application to Clinopyroxene-Bearing Magmas

M. Petrelli[1,2,*], L. Caricchi[3], D. Perugini[1]

[1] Department of Physics and Geology, University of Perugia, IT

[2] INFN, Section of Perugia, IT

[3] Department of Earth Sciences, University of Geneva, CH

Corresponding author: Maurizio Petrelli (maurizio.petrelli@unipg.it)

Key Points:

- Machine learning thermo-barometry is a powerful tool in petrology and volcanology
- Machine learning thermometers and barometers work in a wide compositional range and can be applied independently of tectonic setting
- The most represented magma storage depths in Icelandic volcanoes are in the range 1-5 kbar, with modal values at about 2-3 kbar

This article has been accepted for publication and undergone full peer review but has not been through the copyediting, typesetting, pagination and proofreading process which may lead to differences between this version and the Version of Record. Please cite this article as doi: 10.1029/2020JB020130

Abstract

We introduce a new approach, based on Machine Learning, to estimate pre-eruptive temperatures and storage depths using clinopyroxene-melt pairs and clinopyroxene-only chemistry. The model is calibrated for magmas of a wide compositional range, it complements existing models, and it can be applied independently of tectonic setting. Additionally, it allows the identification of the main chemical exchange mechanisms occurring in response to pressure and temperature variations on the base of experimental data without *a-priori* assumptions. After the validation process, performances are assessed with test data never used during the training phase. We estimate the uncertainty using the Root Mean Square Error (RMSE) and the coefficient of determination (R^2). The application of the best performing algorithm (trained in the range 0-40 kbar and 952-1882 K) to clinopyroxene-melt pairs from primitive to extremely differentiated magmas of both sub-alkaline and alkaline systems returns a RMSE on the order of 2.6 kbar and 40 K for pressure and temperature, respectively. We additionally present a melt- and temperature-independent clinopyroxene barometer in the range 0-40 kbar, characterized by a RMSE of the order of 3 kbar. Tested for tholeiitic compositions in the range 0-10 kbar, the melt- and temperature-independent clinopyroxene barometer has a RMSE of 1.7 kbar. We finally apply the proposed approach to clinopyroxenes from Iceland, providing new, independent, insights about pre-eruptive storage depths of Icelandic volcanoes. The general applicability of this model will promote the comparison between the architecture of plumbing systems across tectonic settings and facilitate the comparison between petrologic and geophysical studies.

Keywords: Machine-Learning; clinopyroxene-melt thermometers; clinopyroxene-melt barometers; clinopyroxene-only barometer, Icelandic magmatism

1 Introduction

Unraveling pre-eruptive temperatures and storage depths of magmas feeding active volcanoes is a fundamental topic in petrology and volcanology (e.g., Devine et al., 1998; Putirka 2008; Putirka 2018). As an example, accurate temperature estimations allow the correct application of diffusion chronometry (e.g., Costa et al., 2020; Petrone et al., 2016; 2018). Also, a reliable definition of pre-eruptive storage depts is mandatory in the characterization of

volcanic plumbing systems (Devine et al., 1998; Kennedy et al., 2018; Petrelli et al., 2018; Ubide & Kamber, 2018).

The development of current geo-thermometers and barometers relies on the modeling of entropy and volume changes occurring in equilibrium reactions between melts and crystals (Putirka, 2018; Putirka, 2008). This approach, based on the thermodynamic characterization of the magmatic system, provides a well-established theoretical framework, and it is widely applied to estimate pre-eruptive magma temperature and storage depths (Masotta et al., 2013; Neave et al., 2019; Nimis, 1995; Nimis and Ulmer, 1998; Putirka, 2008; Putirka et al., 2003). The typical calibration procedure for cpx thermometers and barometers consists in five main steps: a) Identify chemical equilibria associated with large variations of entropy and volume, respectively (Putirka, 2008); b) retrieving a consistent experimental dataset with known T and P (e.g., the LEPR dataset; Hirschmann et al., 2008); c) calculate the cpx components from chemical analyses; d) define a regression strategy; e) model validation (Putirka, 2008).

Several studies reported the calibration of cpx and cpx–melt geothermobarometers in different tectonic settings (Putirka, 2008). The earliest attempts were carried out using a simple system based on cpx only (Nimis, 1995; Nimis & Ulmer, 1998). Although inviting for its simplicity, these early calibrations perform worse than models based on cpx-melt pairs, thus a melt in 'apparent' equilibrium with each investigated crystal is typically required (Neave et al., 2019; Putirka, 2008). Calibrations based on cpx-melt pairs are now widely accepted with advantages, potential pitfalls, and limitations that have been extensively discussed by Putirka (2008). One of the main risks to consider during the calibration procedure of any method is the potential overfitting of the experimental data, which results in poor accuracy in real-world applications (Putirka, 2008). Additionally, many barometers and thermometers can only be applied within a particular, sometimes extremely restricted, range of melt chemistry (i.e., local calibrations; Masotta et al., 2013; Mollo et al., 2018; Neave et al., 2019; Putirka, 2008; Putirka et al., 2003), as they are developed to solve specific problems where generalized calibration fails (Masotta et al., 2013; Mollo et al., 2018; Neave & Putirka, 2017). Finally, the identification of equilibrium crystal-melt pairs is not always trivial, which potentially introduces additional sources of error (Zellmer et al., 2014).

Recently, various studies demonstrated the potentials of Machine Learning (ML) in the solution of petro-volcanological problems (Bolton et al., 2020; Caricchi et al., 2020; Itano et al., 2020; Li et al., 2020; Petrelli et al., 2017; Petrelli & Perugini, 2016; Ren et al., 2019; Ueki et al., 2020). One common feature for ML models is that they do not need to solve complex problems using an *a priori* defined conceptual model (e.g., the definition of a thermodynamic

reaction) but they can follow a data-driven approach (Caricchi et al., 2020; Hazen, 2014; Hazen et al., 2019; Morrison et al., 2017), and unravel complexities in large datasets through a so-called learning process (Shai & Shai, 2014).

In the present study, we test the potentials of Machine Learning approaches to be used as thermometers and barometers. In detail, we report on the development of cpx and cpx-melt thermometers and barometers in a wide range of P-T-X conditions using Machine Learning (ML) algorithms. We define a strategy to avoid overfitting and demonstrate the robustness of the calibrated models over a wide range of chemical compositions of the melt phase (i.e., a generalized calibration). We compare the performance of ML algorithms with classical and established calibrations of cpx based thermometers and barometers. We finally present a temperature-independent, cpx only barometer that we apply and discuss in the framework of Icelandic magmatism providing new and independent insights about the architecture of the Barðarbunga volcanic plumbing systems.

2 Material and Methods

2.1 Experimental dataset

The global dataset used for the present study consists of a 1403 experimentally produced clinopyroxenes in equilibrium with a wide range of silicate melt compositions (Tab. S1; Fig. 1) at pressures and temperatures in the range 0.001-40 kbar and 952-1883 K, respectively (a detailed description of the dataset has been reported as Supplementary Material, Text S1). As input parameters, we used the major element compositions of melt (SiO_2, TiO_2, Al_2O_3, FeOt, MnO, MgO, CaO, Na_2O, K_2O, Cr_2O_3, P_2O_5, H_2O) and clinopyroxene (SiO_2, TiO_2, Al_2O_3, FeOt, MnO, MgO, CaO, Na_2O, K_2O, Cr_2O_3) phases. Data below the detection limits were reported as 0 wt %. The system was considered anhydrous (i.e., H_2O = 0 wt%) when H_2O was not explicitly reported. The dataset is a collection of literature data and it is reported as Supplementary material (Table S1; Text S1).

2.2 Data Standardization

Standardization of the dataset is a common requirement for many machine-learning estimators. In the present study, we transformed the original dataset by removing the mean and scaling to unit variance:

$$\tilde{x}_i^e = \frac{x_i^e - \mu^e}{\sigma^e}$$

where $\tilde{x}_i^e$, x_i^e are the transformed and the original value of each component belonging to the population of the chemical analyses of the element *el* (i.e., SiO_2, TiO_2, etc…), characterized by an average μ^e and a standard deviation σ^e.

2.3 Classic regression and Machine Learning algorithms

We use six different algorithms: Ordinary least squares Linear Regression (Montgomery et al., 2012) plus ML-based Stochastic Gradient Boosting (Friedman, 2002), Extremely Randomized Trees (ERT, Geurts et al., 2006), Random forests (Breiman, 2001), k-nearest neighbors (Bentley, 1975), and decision trees (Breiman et al., 1984) regressions. We report a detailed description of the principles behind each algorithm as Supplementary Material (Text S2). We selected these six algorithms for two main reasons: 1) they are all well established and widely used in literature, 2) they are all based on rules that follow the "wisdom of the crowds" idea or a simple mathematical expression of similarity (k-nearest neighbors), making them easily comprehensible to non experts. We used the scikit-learn implementation for both classic regression and Machine Learning algorithms (Pedregosa et al., 2011). Scikit-learn is a Python open-source library that supports supervised and unsupervised learning (https://scikit-learn.org/ - Pedregosa et al. 2011). This package focuses on bringing machine learning to non-specialists using a general-purpose high-level language (Pedregosa et al. 2011). We selected to use the scikit-learn package as this will allow other users to easily replicate our results. In addition, it represents a powerful framework for the solution of petrological and mineralogical problems in fields of clustering, classification, dimensionality reduction, and regression (Petrelli & Perugini, 2016).

2.4 Strategies and Metrics

The goodness of the results has been evaluated coupling two parameters: the coefficient of determination and the root mean squared error metrics. The combination of these two metrics, associated with a robust procedure to avoid the overfitting of the input data, provides

a widely recognized strategy to evaluate the goodness of predictions in regression analyses (Branco et al., 2016).

Coefficient of determination (R^2): It provides an indication of goodness of fit and therefore a measure of how well unknown samples are likely to be predicted by the model:

$$R^2 = 1 - \frac{\sum_{i=1}^{n}(y_i - \hat{y}_i)^2}{\sum_{i=1}^{n}(y_i - \bar{y})^2}$$

where $\hat{y}_i$ and y_i are the predicted and the expected values respectively, and $\bar{y} = \frac{1}{n}\sum_{i=1}^{n} y_i$. The best possible score for R^2 is 1.0 and can also assume negative values. In detail R^2 scores outside the range from 0 to 1 can occur when the selected algorithm fits the data worse than a horizontal hyperplane, meaning that utilized regressor is not suitable to model the studied problem.

Root Mean Squared Error (RMSE): it is the square root of the sum of all errors divided by the number of values:

$$RMSE = \sqrt{\frac{\sum_{i=1}^{n}(y_i - \hat{y}_i)^2}{n}}$$

RMSE is the equivalent of Standard Error of Estimate (SEE), and it is characterized by the same physical unit of the investigated parameter, in our case K and kbar for temperature and pressure, respectively. *RMSE* is always non-negative with a value of 0 indicating a perfect fit to the data, corresponding to an ideal R^2 value equal to 1. In detail, the *RMSE* and R^2 values are both a measure of the 'prediction ability' of a regression method, with the first providing a dimensional estimate of the errors associated with a prediction, and the second measuring the goodness of correlation between expected and predicted values.

Dataset balancing and training of the ML algorithm: To avoid potential accuracy biases due to training of the ML algorithm using a target unbalanced dataset, we inspected the P and T histogram distributions and, following the suggestion provided by Branco et al. (2016), we randomly subsampled majority (i.e., oversampled) classes. In detail, we resampled the dataset using a binning of 2 kbar and we randomly removed samples form the classes that were over-represented. In our case the class with most experiments was 0 to 2 kbar. The comparison between the calibration performed using the unbalanced and the balanced dataset shows that

the unbalance dataset tends to underestimate the pressure by 0.5 kbar. Hence the relative effect of using the balance vs the total dataset is less important with the increase of the pressure estimates. Also, similar tests should be performed by the users (of any thermo-barometer) when working on magma chemistries that are extreme with respect to the compositions within the calibration dataset. We reported the balanced dataset, which is the only one we have used throughout the article, in Table S2 and Figure 1B and 1C. As a first step, 119 experiments (Tab. S4) were removed from the balanced dataset and never used during the training process to test the predictive performance of the ML algorithms (test dataset). The remaining data (Tab. S3) were randomly split in two portions: one sub-dataset (70%) was used for training (i.e., train dataset) and the second (30%) for validating (i.e., validation dataset) the P and T predictions. We suggest to follow the approaches described here to reduce overfitting and produce unbiased performance tests for any model and not only when using machine learning.

Robustness of the provided results: To provide a robust performance estimation of each ML algorithm, we performed n=1000 replications of the random splitting, training, and validation procedures and analysed the distributions of R^2 and RMSE.

Feature relative importance: In Extremely Randomized Trees (Geurts et al., 2006) and Random forests (Breiman, 2001) methods, the rank of a feature used as a decision node in a tree can be used to evaluate its relative importance with respect to the predictability of the target variable (Louppe at al., 2013). More precisely, the features used at the top of a tree contribute to the final prediction decision to a larger extent than those at lower levels (Louppe at al., 2013). To estimate the 'feature relative importance, the scikit-learn implementation (Pedregosa et al. 2011), utilizes the Mean Decrease in Impurity (MDI) procedure (Louppe at al., 2013).

2.5 Cpx-melt Thermometers and Barometers from Literature

To validate the robustness of our approach, we compare the results obtained applying ML algorithms to pressure and temperature estimation on cpx-melt pairs, with those obtained using the equations reported by Neave and Putirka (2017), Putirka (2008), and Putirka et al. (2003). These equations are only applicable in specific ranges of melt composition. Putirka et al. (2003) calibrated two equations (i.e., Model A for pressure and Model B for temperature) on the basis of a jadeite crystallization and jadeite-diopside plus hedenbergite (Jd-DiHd) exchange equilibria for sub alkaline, mafic to evolved, volatile-bearing lava compositions in

the pressure and temperature ranges of 0-40 kbar and 1200-2100 K, respectively. Equation 33 by Putirka (2008) expand the Jd-DiHd calibrations to a larger span of P experiments conducted up to P < 70 kbar. The Equation 32c by Putirka (2008) is a barometer based on the partitioning of Al between clinopyroxene and melt. Finally, Neave and Putirka (2017), calibrated a Jd-in-clinopyroxene equation for P estimation in the 1 atm to 20 kbar range to improve the accuracy of P estimations of tholeiites at pressures relevant to magma storages at crustal levels.

The above-reported equations for P and T estimations based on cpx-melt pairs are only a part of the many different calibrations that have been reported in the literature (Masotta et al., 2013; Neave et al., 2019; Neave & Putirka, 2017; Nimis, 1995; Nimis & Ulmer, 1998; Putirka, 2008; Putirka et al., 2003). However, they represent a comprehensive set of equations to assess performances and the generalization capabilities of the algorithms we present here.

3 Results

Figures 2A reports the R^2 probability density distributions for pressure estimations performed on the validation dataset in the range 0.001- 40 kbar using six ML algorithms on cpx-melt pairs chemical compositions (i.e., 22 features, 12 major elements for the silicate melt and 10 major elements for the clinopyroxenes). Extremely Randomized Tree regression technique (Geurts et al., 2006) is the best performing ML algorithm, with a R^2 probability density distribution characterized by a modal value equal to 0.91 and a RMSE value of 2.6 kbar (Fig. 2A). The modal R^2 of other ML algorithms presented here ranges between 0.7 and 0.9, with the RMSE of 3-4.4 kbar. To compare the performance of the ERT algorithm we consider two well-established calibrations (Fig. 2B; Putirka, 2008; Putirka et al., 2003). Within the same compositional ranges of the melt phase provided by the authors, and with an accurate knowledge of the temperature, the R^2 of these models are comparable to those of the ERT algorithm (Fig. 2B). However, the ERT algorithm performs better on the entire validation datasets, which implies that it can be applied to cpx from magmas of a wider compositional range and without *a-priori* knowledge of the investigated temperatures (Fig. 2B). Finally, we test the capacity of the different ML algorithms to predict pressure using exclusively cpx chemistry (i.e., 10 features only; Fig. 2C). ERT remains the best performing among the investigated ML algorithms, with a modal R^2 equal to 0.88 and a RMSE equal to 3.2 kbar. Importantly, the predictive capacity of this algorithm does not deteriorate significantly by removing the melt chemistry from the training features (Fig. 2A, C).

Figures 3A reports the R^2 probability density distribution for thermometry in the range 952-1883 K using the six ML algorithms on cpx-melt pairs (i.e., 22 features). As for the pressure estimates, the Extremely Randomized Trees regression technique shows the best distribution of R^2, with a modal value of 0.94 and a RMSE equal to 40 K (Fig. 3A). Also, the comparison with the equation 33 reported by Putirka (2008) highlights that: a) the equation 33 shows the same predictive capabilities of the ERT model within the constraints reported by Putirka (2008), b) the ERT model perform better when working with the entire validation dataset, indicating a superior generalization capability, i.e. applicable on a wider compositional range with respect to existing calibrations. Using exclusively cpx chemistry (i.e. 10 features) to predict temperature leads to a general decrease of the performance of all ML algorithms, however, ERT remains the best performing ML algorithm with a R^2 probability density distribution characterized by a modal value of 0.83 and a RMSE equal to 66 K (Fig. 3C).

To better visualize the predictive performances of the ERT for pressure (Fig. 4A) and temperature (Fig. 4B) using clinopyroxene-melt pairs, Figure 4 shows the results of one of the 1000 P-T estimates obtained for the validation datasets, and used to generate the R^2 probability density distributions reported in Figures 2 and 3. In the diagrams of Figure 4, the results of a model that perfectly predicts the expected values, will lie on a one to one straight line (black lines in Fig. 4).

The good pressure and temperature predictive performances of the ERT is confirmed by its application to the test dataset, which was never used during the training and validation phase (Supplementary Tab.4; Figs. 5, 6). Figures 5 and 6 highlight R^2 scores for the ERT algorithm of 0.94 for both pressure and temperature estimates with RMSEs of 2.9 kbar (Fig. 5A) and 51 K (Fig. 6A), respectively. Also, figure 5 reports the R^2 and RMSE scores obtained by the application the Eq.32c (Putirka, 2008) and the calibration proposed by Neave and Putirka (2017) on the test dataset. Finally, Figure 6B shows the R^2 and RMSE scores for the Eq.33 (Putirka, 2008) on the test dataset.

4 Discussion

4.1 Capacity of Machine-Learning to estimate pre-eruptive pressures and temperatures

Our results indicate that the ML approach we propose provides estimates for both pressure and temperature that are comparable to existing model but applicable over a wider compositional range. The main elements controlling the predictive capacity of our ERT are

Al_2O_3, Na_2O, CaO content of cpx and MgO of the melt and MgO, CaO, FeOt of the melt, for pressure and temperature, respectively (Fig. 7). Thus, pressure information in pyroxene-bearing magmas are mainly stored in Na_2O, Al_2O_3, and CaO in pyroxene with an important contribution of MgO in the melt (Fig. 7A). This explains why the capacity of the algorithm to predict pressure decreases (from 0.91 to 0.88) when not taking into account the chemistry of the melt phase. The reported results are in agreement with previous studies relating pressure and temperature changes to cpx chemistry (e.g., Gaetani, 2004; Putirka, 2008). As an example, it is well known tha Na, Al and Ca in cpx are strogly affected by pressure variations (e.g., Gaetani, 2004; Nimis, 1995; Nimis and Ulmer 1998; Putirka, 2008). The dominant control of MgO, CaO, and FeO in the melt on the temperature estimates is also not surprising, and is in agreement with thermodynamic methods based on the melt phase only (Helz & Thornber, 1987; Montierth et al., 1995; Putirka, 2008; Thornber et al., 2003). The strong control of these elements also accounts for the significant drop in the capacity of the algorithm to predict temperature when using only cpx chemistry (R^2 from 0.94 to 0.83). Summarizing, Figure 7 higlights that, in agreement with previous studes (e.g., Gaetani 2004; Nimis and Ulmer 1998), pressure and temperature changes are mainly recoded by cpx and melt, respectively. However, coupling the informations stored in both the cpx and melt phases, the predictive capability of the ERT model increases since both the crystal and melt structure exert an important control on element partitioning as response of temperature and pressure changes (e.g., Gaetani, 2004; Putirka, 2008).

We show that a ML approach improves the performance of thermo-barometers over the full range of pressure and temperature investigated (Figs. 3, 4). Our interpretation of these improved performances relies on simple but significant evidence: current methods are based on chemical exchanges models considering pure end-members components (i.e., Augite, Diopside, Hedenbergite, and Jadeite). While it is demonstrated that the crystallographic structure and chemistry of cpx changes in response to pressure or temperature (Nimis and Ulmer, 1998), it is clear that the assumption of end-member purity cannot fully capture the relationships between cpx chemistry and intensive parameters such as pressure and temperature especially when dealing with natural material (i.e. underfitting). ML methods do not rely on any assumption and can also capture compositional variations of cpx not directly linked to pressure or temperature. As an example, Cr is generally not included in current models because it does not vary directly in response to P and T changes. However, Figure 7 shows that Cr content in the liquid phase is a feature of average importance to recalculate P and T, thus not including it, will have a detrimental effect on the predictive capacity of our model. The relative

importance of Cr is very likely a consequence of its compatibility during magma fractionation, with high Cr concentration indicating generally high pressure and/or temperature of cpx crystallisation (Ishii et al., 1992). However, when using ML algorithms and in general models involving many elements that are non-linearly related, the issue of overfitting must be addressed carefully (Putirka, 2008), as explained in the method section.

On the other hand, existing calibrations seem performing better in specific compositional ranges. As an example, Masotta et al. (2013) reported SEE of the order of 1.15 kbar and 18 K, for phonolitic and trachytic melts between 0 and 15 kbar and a temperature range of 300 K, respectively. Extending the compositional range to tephritic-phonolite and phonolitic-tephrite melts, the SEE increase from 1.15 to 3.4 kbar (Masotta et al., 2013). Neave and Putirka (2017) reported a calibration for pressure estimations of anhydrous tholeiitic magmas with SEE of 1.4 kbar.

To test the performance of ERT on specific compositional field of the melt phase, we compared its performance with those of the calibration proposed by Neave and Putirka, (2017). In particular, we utilized the same test dataset for Tholeiites reported in Appendix 1 by Neave and Putirka (2017). Then, following Neave and Putirka (2017), we train the ERT algorithm excluding all data reported in the test dataset for Tholeiites and data from Yang et al. (1996), Villiger et al. (2007, 2004), Grove et al. (1992), and Yang et al. (1996). Figure 8A, 8B show the results derived by the application of the ML technique to the test dataset for Tholeiites on the cpx-melt pairs and clinopyroxenes only, respectively. The results of the calibration proposed by Neave and Putirka (2017) are also reported in Figure 8C. The application of the ERT algorithm on cpx-melt pairs (Fig. 8A) returns a RMSE of 1.5 kbar, and a R^2 of 0.78. Training the ML algorithm using the clinopyroxene composition only, the RMSE rises to 1.7 kbar, with a regression line characterized by a R^2 fo 0.73 (Fig. 8B). These results are in statistical agreement with those obtained by Neave and Putirka (2017; Fig. 8C) indicating that the performance of the ERT is comparable to other calibrations in restricted pressure and compositional ranges. The results reported in Figure 8 further demonstrate the good performance of ML algorithm both when dealing with the global dataset and with specific compositions of the melt phase.

The evidence that pyroxenes stores most of the information about pressure, motivated us to further investigate the capacity of the ERT based exclusively on cpx chemistry. Using a full clinopyroxene based, melt-free, and temperature-independent barometer (i.e., only based on the clinopyroxene major element composition), although characterized by larger RMSEs, has some significant advantages over the application of pressure estimators based on crystal-

melt pairs. The most significant is that, finding a melt composition that is in equilibrium with each studied clinopyroxene is often challenging, and entails additional uncertainty on pressure estimates (that are generally not propagated).

In some cases, textural relationships between crystals and their carrier melts (i.e., matrix glasses) suggest that these two phases were in equilibrium at the time of quenching (Neave & Putirka, 2017). Also, tests to check for the equilibrium between crystals and melts have been developed (Mollo et al., 2013; Putirka, 1999). However, it is not always easy to find the 'right' melt in equilibrium with the analysed clinopyroxenes. To overcome this limitation, iterative equilibrium melt-matching strategies have been proposed (Neave et al., 2019; Neave & Putirka, 2017; Winpenny & Maclennan, 2011). An efficient solution to estimate the error associated with a wide range of melt chemistries in apparent equilibrium with the studied cpx crystals was proposed by Neave et al. (2019) for a study of the Holuhraun-Bárðarbunga eruption (Iceland). All cpx-melt pairs in apparent equilibrium were used to provide a pressure estimate allowing error propagation and highlighting an additional 1-sigma errors associated with this procedure of up to 0.84 kbar (Neave et al., 2019). We follow this approach and report in Figure 9A all the Icelandic magma compositions available in the Georoc database (georoc.mpch-mainz.gwdg.de/). To provide an estimate of the error associated with the procedure adopted for the selection of cpx-melt pairs in equilibrium with a single cpx, we identify those compositions in apparent equilibrium with the cpx composition '292' reported by Neave and Putirka (2017) from the Laki eruption. We accepted as in 'apparent equilibrium' all the cpx-melt pairs passing the criteria reported by Neave et al. (2019). Then, we calculated the pressures using the calibration reported by Neave and Putirka (2017). We estimated a supplemental uncertainty, associated with selecting the equilibrium melt composition, of the order of 1.2 kbar (2-sigma; Fig. 9B). Such additional source of uncertainty is absent in cpx-only calibrations, indipendenlty of the adopted calibration, either classical or based on ML. However, this does not remove the assumption of equilibrium crystallization for cpx, which if not addressed would result in pressure estimate that could be profoundly incorrect (Mollo et al., 2013; Neave et al., 2019; Putirka, 2008). In theory, ML methods could be trained to identify and deal with non-equilibrium systems, however, the dataset of non-equilibrium experiments is still not mature enough to successfully develop statistically robust calibrations. Also, analytical biases must be avoided (Neave & Putirka, 2017; Putirka, 2008). As a consequence, a strategy to ensure that pressure estimations are based only on clinopyroxenes crystallising at or near equilibrium is still mandatory. To avoid analytical biases we suggest following the approach of Neave and Putirka (2017): a) removal of all analyses that results in non-stoichiometric cpx chemical

formula; b) exclusion of analyses with a Jadeitic component lower than 0.01, which represent Na_2O contents at or below the detection limit of EPMA. Regarding the equilibrium assumption, we suggest starting with petrographic observations of the analysed crystals. Also, we suggest ensuring in the system at least one melt composition in 'apparent equilibrium' with the studied clinopyroxenes, following the procedure reported by Neave et al. (2019).

4.2 Application of the cpx only ERT barometer to Icelandic volcanoes

The results reported by Neave et al. (2019, 2015) and Neave and Putirka (2017), show that most of the current cpx-melt barometers seem to overestimate storage pressures when applied to Icelandic magmas. In the specific case of H_2O-poor tholeiites, Neave and Putirka (2017) reported substantial pressure-dependent inaccuracies by commonly used clinopyroxene-liquid barometers when applied on experimental data in the 0.001-10 kbar, with some models overestimating pressures of experimental products of about 3 kbar (i.e., ~ 12 km). As a consequence, Neave and Putirka (2017), developed a new calibration, specific for tholeiitic compositions.

To test our calibration on Icelandic magma feeding systems, we start applying the cpx-only ERT algorithm to the same dataset of natural samples used in Neave and Putirka (2017; Fig. 10). This comparison highlights a general agreement between the ERT estimates and those based on the calibration reported by Neave and Putirka (2017). In detail, crystallization pressure distributions are mostly in the range 0-5 kbar for Holuhraun 1-2, Laki, Saksunarvatn, and Skuggafjoll. Thjorsa and Borgarhraun system highlight pressure estimates in the range 0-6 and 1-11 kbar, respectively. The application of the cpx only ERT barometer to the data reported by Caracciolo et al. (2020) for eruptions ranging from ~100 ka to 1477 AD in the Barðarbunga volcanic system (Iceland), returns crystallization pressures in the range 0-5 kbar, with an average value of 2.1 ± 0.9 kbar (Fig 11A). The obtained estimates are in agreement with clinopyroxene-melt (Neave & Putirka, 2017) and olivine–plagioclase–augite–melt (Hartley et al., 2018) barometry, returning crystallization pressures of 2.2 ± 0.7 (1s) and 1.9 ± 0.8 (1s) kbar, respectively (Caracciolo et al., 2020). Crystallization pressure estimates by the ERT barometer also agree with those reported in Figure 10A (2.0 ± 0.5 kbar), for the Holuhraun 1-2 eruptions, dated 797 and 1862–1864, respectively (Hartley & Thordarson, 2013).

Additionally, we apply the cpx only ERT barometer to the analyses reported by Caricchi et al. (2020) and Geiger et al. (2016) for the 2014-15 Holuhraun eruption (Barðarbunga volcanic system; Fig. 11A). Observing Figure 11, it emerges that: 1) clinopyroxenes registered crystallization pressures mostly in the range 1-6 kbar; 2) combining

all pressure estimates (Fig. 11B), the pressure range with the highest probability (i.e., 74 %) is 1-3 kbar; 3) the average of all pressure estimations for the Barðarbunga volcanic system by the ERT barometer is 2.3 ± 1.1 kbar. Summarizing, crystallization pressure estimates by the cpx-only, melt- and temperature-independent ERT barometer point to a distribution in the range 1-6 kbar with temporally persistent (i.e., last 100 ka), final magma storage zone in the range 1-3 kbar. These results are in agreement with those reported by Caracciolo et al. (2020), Halldórsson et al. (2018) and Neave et al. (2019) and are consistent with geophysical observations (Hartley et al., 2018). In the attempt to complement these results and provide a generalize interpretation, we extend the application of the ERT barometer to a larger dataset of Icelandic cpx compositions. In detail, we selected all crystals hosted in volcanic rocks from basaltic to rhyolitic compositions erupted by Icelandic volcanoes and reported in the Georoc dataset (georoc.mpch-mainz.gwdg.de/). We discarded non stochiometric analyses and those resulting in Jd compositions lower than 0.01. Also, we checked the 'apparent equilibrium' by matching cpx compositions with those of whole rock by the Georoc database belonging to the area of interest. Observing the probability distributions reported in Figure 12A, it emerges that the most represented pressure range is 1-5 kbar, with a probability of occurrence close to 85 %, and a modal value at 2.3 kbar. Also, the density distribution show a tail at higher pressures, registering values up to 25 kbar. Assuming an average crustal density of 2800 kg/m^3 (Tarasewicz et al., 2012), the probability density distribution of Figure 12A highlights a strong probability for magma storages at crustal levels between 2.5 and 14 km, with depths as high as 70 km. Clinopyroxenes crystallized in magmas of different chemistry show that that the deepest pressures are registered by basaltic magmas (Figure 12B). This is not surprising and it support the idea reported in Figure 13, depicting crustal magmatic reservoirs (i.e., stored at pressures below 5 kbar) fed by primitive magmas from deeper levels (i.e., about 25 kbar, corresponding to about 70 km; Fig. 13). Also, our estimates suggest that more chemically evolved magmas are stored at pressures below 7 kbar (i.e., less than 20 km; Fig. 12 C, D), mostly in the range 1-5 kbar (i.e., 2.5 and 14 km), with modal values at about 2-4 kbar (5.5 and 10 km; Fig. 13).

5 Conclusions

We reported a new approach based on Machine-Learning (ML) to estimate pre-eruptive temperatures and pressures. The approach does not assume any *a-priori* knowledge of chemical exchange between the crystal and the carrier melt. Our results highlight that the ML approach can be applied on a much wider compositional range than existing models. It complements existing calibrations and can be used as an independent tool, also to validate the results obtained

by current models based on the thermodynamic of the system. Additionally, we present a ML barometer based exclusively on clinopyroxene (cpx) chemistry that we show performs well in the challenging case of Iceland, where a general overestimation of magma storage depths by currently established cpx-melt barometers, recently required the development of a specific calibration. The use of a barometer based exclusively on clinopyroxene instead of cpx-melt pair, although characterized by slightly higher RMSE when applied to experimental data, has the important advantage of not requiring the knowledge of the equilibrium melt composition, which removes the error associated with cpx-melt equilibrium pairing.

Being suitable to investigate a large spread of chemical compositions, we discussed the crystallization depths of cpxs hosted in magmas of different compositions, better constraining the nature of volcanic plumbing systems below Icelandic volcanoes. The wide range of magma chemistry to which the reported method is applicable allows for the comparison of the architecture of plumbing systems across tectonic settings and provides an additional approach to to compare pre-eruptive magma storage conditions obtained by geophysics and petrology.

Acknowledgments

MP acknowledge the Università degli Studi di Perugia FRB2019 grant "ENGAGE – machinE learNinG Applications for Geological problEms." LC received funding from the European Research Council (ERC) under the European Union's Horizon 2020 research and innovation programme (grant agreement No. 677493-FEVER).

Data Availability

Python scripts for the application of ML thermo-barometry are available in Zenodo at the following url: https://zenodo.org/record/3972790#.X0v7Mi1h2L8

References

Almeev, R. , Holtz, F., Koepke, J., Parat, F., & Botcharnikov, R. E. (2007). The effect of H_2O on olivine crystallization in MORB: Experimental calibration at 200 MPa. *American Mineralogist*, *92*(4), 670–674. https://doi.org/10.2138/am.2007.2484

Andújar, J., Costa, F., Martí, J., Wolff, J. A. A., & Carroll, M. R. R. (2008). Experimental constraints on the pre-eruptive conditions of the phonolitic magma from the caldera-forming the Abrigo eruption, Tenerife (Canary Islands). *Chemical Geology*, *257*(3–4), 173–191. https://doi.org/10.1016/j.chemgeo.2008.08.012

Andújar, J., Costa, F., & Martí, J. (2010). Magma storage conditions of the last eruption of

Teide volcano (Canary Islands, Spain). *Bulletin of Volcanology*, *72*(4), 381–395. https://doi.org/10.1007/s00445-009-0325-3

Andújar, Joan, & Scaillet, B. (2012). Relationships between pre-eruptive conditions and eruptive styles of phonolite-trachyte magmas. *Lithos*, *152*, 122–131. https://doi.org/10.1016/j.lithos.2012.05.009

Baker, D. R., & Eggler, D. H. (1987). Compositions of anhydrous and hydrous melts coexisting with plagioclase, augite, and olivine or low-Ca pyroxene from 1 atm to 8 kbar: application to the Aleutian volcanic center of Atka. *American Mineralogist*, *72*(1–2), 12–28.

Baker, M. B., Grove, T. L., & Price, R. (1994). Primitive basalts and andesites from the Mt. Shasta region, N. California: products of varying melt fraction and water content. *Contributions to Mineralogy and Petrology*, *118*(2), 111–129. https://doi.org/10.1007/BF01052863

Barclay, J., & Carmichael, S. E. (2004). A hornblende basalt from western Mexico: Water-saturated phase relations constrain a pressure-temperature window of eruptibility. *Journal of Petrology*, *45*(3), 485–506.

Bartels, K. S., Kinzler, R. J., & Grove, T. L. (1991). High pressure phase relations of primitive high-alumina basalts from Medicine Lake volcano, northern California. *Contributions to Mineralogy and Petrology*, *108*(3), 253–270. https://doi.org/10.1007/BF00285935

Bender, J. F., Hodges, F. N., & Bence, A. E. (1978). Petrogenesis of basalts from the project FAMOUS area: experimental study from 0 to 15 kbars. *Earth and Planetary Science Letters*, *41*(3), 277–302. https://doi.org/10.1016/0012-821X(78)90184-X

Bentley, J. L. (1975). Multidimensional binary search trees used for associative searching. *Communications of the ACM*, *18*(9), 509–517. https://doi.org/10.1145/361002.361007

Blatter, D. L., Sisson, T. W., & Hankins, W. B. Ben. (2013). Crystallization of oxidized, moderately hydrous arc basalt at mid- to lower-crustal pressures: Implications for andesite genesis. *Contributions to Mineralogy and Petrology*, *166*(3), 861–886. https://doi.org/10.1007/s00410-013-0920-3

Bolton, M. S. M., Jensen, B. J. L., Wallace, K., Praet, N., Fortin, D., Kaufman, D., & De Batist, M. (2020). Machine learning classifiers for attributing tephra to source volcanoes: an evaluation of methods for Alaska tephras. *Journal of Quaternary Science*, *35*(1–2), 81–92. https://doi.org/10.1002/jqs.3170

Botcharnikov, R. E., Almeev, R., Koepke, J., & Holtz, F. (2008). Phase relations and liquid

lines of descent in hydrous ferrobasalt - Implications for the skaergaard intrusion and Columbia river flood basalts. *Journal of Petrology*, *49*(9), 1687–1727. https://doi.org/10.1093/petrology/egn043

Branco, P., Torgo, L., & Ribeiro, R. P. (2016). A survey of predictive modeling on imbalanced domains. *ACM Computing Surveys*, *49*(2). https://doi.org/10.1145/2907070

Breiman, L. (2001). Random forests. *Machine Learning*, *45*(1), 5–32. https://doi.org/10.1023/A:1010933404324

Breiman, L. (1996). Bagging Predictors. Machine Learning, 24(2), 123–140. https://doi.org/10.1023/A:1018054314350

Breiman, L., Friedman, J. H. Jerome H. ., Olshen, R. A., & Stone, C. J. (1984). *Classification and regression trees*. Chapman and Hall/CRC. ISBN: 9781138469525

Bulatov, V. K., Girnis, A. V., & Brey, G. P. (2002). Experimental melting of a modally heterogeneous mantle. *Mineralogy and Petrology*, *75*(3–4), 131–152. https://doi.org/10.1007/s007100200021

Caracciolo, A., Bali, E., Guðfinnsson, G. H., Kahl, M., Halldórsson, S. A., Hartley, M. E., & Gunnarsson, H. (2020). Temporal evolution of magma and crystal mush storage conditions in the Bárðarbunga-Veiðivötn volcanic system, Iceland. *Lithos*, *352–353*. https://doi.org/10.1016/j.lithos.2019.105234

Caricchi, L., Petrelli, M., Bali, E., Sheldrake, T., Pioli, L., & Simpson, G. (2020). A Data Driven Approach to Investigate the Chemical Variability of Clinopyroxenes From the 2014–2015 Holuhraun–Bárdarbunga Eruption (Iceland). *Frontiers in Earth Science*, *8*. https://doi.org/10.3389/feart.2020.00018

Conte, A. M., Dolfi, D., Gaeta, M., Misiti, V., Mollo, S., & Perinelli, C. (2009). Experimental constraints on evolution of leucite-basanite magma at 1 and 10^{-4} GPa: Implications for parental compositions of Roman high-potassium magmas. *European Journal of Mineralogy*, *21*(4), 763–782. https://doi.org/10.1127/0935-1221/2009/0021-1934

Costa, F., Shea, T., & Ubide, T. (2020). Diffusion chronometry and the timescales of magmatic processes. *Nature Reviews Earth & Environment*, *1*(4), 201–214. https://doi.org/10.1038/s43017-020-0038-x

Dann, J. C., Holzheid, A. H., Grove, T. L., & McSween, H. Y. (2001). Phase equilibria of the Shergotty meteorite: Constraints on pre-eruptive water contents of martian magmas and fractional crystallization under hydrous conditions. *Meteoritics and Planetary Science*, *36*(6), 793–806. https://doi.org/10.1111/j.1945-5100.2001.tb01917.x

Devine, J. D., Murphy, M. D., Rutherford, M. J., Barclay, J., Sparks, R. S. J., Carroll, M. R.,

et al. (1998). Petrologic evidence for pre-eruptive pressure-temperature conditions, and recent reheating, of andesitic magma erupting at the Soufriere Hills Volcano, Montserrat, W.I. *Geophysical Research Letters*, *25*(19), 3669–3672

Di Carlo, I., Pichavant, M., Rotolo, S. G., & Scaillet, B. (2006). Experimental crystallization of a high-K arc basalt: The golden pumice, Stromboli volcano (Italy). *Journal of Petrology*, *47*(7), 1317–1343. https://doi.org/10.1093/petrology/egl011

Draper, D. S., & Green, T. H. (1999). P-T phase relations of silicic, alkaline, aluminous liquids: New results and applications to mantle melting and metasomatism. *Earth and Planetary Science Letters*, *170*(3), 255–268. https://doi.org/10.1016/S0012-821X(99)00111-9

Draper, D. S., & Johnston, A. D. (1992). Anhydrous PT phase relations of an Aleutian high-MgO basalt: an investigation of the role of olivine-liquid reaction in the generation of arc high-alumina basalts. *Contributions to Mineralogy and Petrology*, *112*(4), 501–519. https://doi.org/10.1007/BF00310781

Dunn, T., & Sen, C. (1994). Mineral/matrix partition coefficients for orthopyroxene, plagioclase, and olivine in basaltic to andesitic systems: A combined analytical and experimental study. *Geochimica et Cosmochimica Acta*, *58*(2), 717–733. https://doi.org/10.1016/0016-7037(94)90501-0

Elkins-Tanton, L. T., & Grove, T. L. (2003). Evidence for deep melting of hydrous metasomatized mantle: Pliocene high-potassiuim magmas from the Sierra Nevadas, *108*(7).

Elkins-Tanton, L. T., Draper, D. S., Agee, C. B., Jewell, J., Thorpe, A., & Hess, P. C. (2007). The last lavas erupted during the main phase of the Siberian flood volcanic province: Results from experimental petrology. *Contributions to Mineralogy and Petrology*, *153*(2), 191–209. https://doi.org/10.1007/s00410-006-0140-1

Fabbrizio, A., & Carroll, M. R. (2008). Experimental constraints on the differentiation process and pre-eruptive conditions in the magmatic system of Phlegraean Fields (Naples, Italy). *Journal of Volcanology and Geothermal Research*, *171*(1–2), 88–102. https://doi.org/10.1016/j.jvolgeores.2007.11.002

Falloon, T. J., & Danyushevsky, L. V. (2000). Melting of refractory mantle at 1·5, 2 and 2·5 GPa under anhydrous and H_2O-undersaturated conditions: Implications for the petrogenesis of high-Ca boninites and the influence of subduction components on mantle melting. *Journal of Petrology*, *41*(2), 257–283.

Falloon, T. J., Green, D. H., O'Neill, H. S. C., & Hibberson, W. O. (1997). Experimental

tests of low degree peridotite partial melt compositions: Implications for the nature of anhydrous near-solidus peridotite melts at 1 GPa. *Earth and Planetary Science Letters*, *152*(1–4), 149–162.

Falloon, T. J., Green, D. H., Danyushevsky, L. V., & Faul, U. H. (1999). Peridotite melting at 1·0 and 1·5 GPa: An experimental evaluation of techniques using diamond aggregates and mineral mixes for determination of near-solidus melts. *Journal of Petrology*, *40*(9), 1343–1375. https://doi.org/10.1093/petroj/40.9.1343

Falloon, T. J., Danyushevsky, L. V., & Green, D. H. (2001). Peridotite melting at 1 GPa: Reversal experiments on partial melt compositions produced by peridotite-basalt sandwich experiments. *Journal of Petrology*, *42*(12), 2363–2390.

Feig, S. T., Koepke, J., & Snow, J. E. (2006). Effect of water on tholeiitic basalt phase equilibria: An experimental study under oxidizing conditions. *Contributions to Mineralogy and Petrology*, *152*(5), 611–638. https://doi.org/10.1007/s00410-006-0123-2

Feig, S. T., Koepke, J., & Snow, J. E. (2010). Effect of oxygen fugacity and water on phase equilibria of a hydrous tholeiitic basalt. *Contributions to Mineralogy and Petrology*, *160*(4), 551–568. https://doi.org/10.1007/s00410-010-0493-3

Fram, M. S., & Longhi, J. (1992). Phase equilibria of dikes associated with Proterozoic anorthosite complexes. *American Mineralogist*, *77*(5–6), 605–616.

Freda, C., Gaeta, M., Palladino, D. M., & Trigila, R. (1997). The Villa Senni Eruption (Alban Hills, central Italy): The role of H_2O and CO_2 on the magma chamber evolution and on the eruptive scenario. *Journal of Volcanology and Geothermal Research*, *78*(1–2), 103–120. https://doi.org/10.1016/S0377-0273(97)00007-3

Freda, C., Gaeta, M., Misiti, V., Mollo, S., Dolfi, D., & Scarlato, P. (2008). Magma-carbonate interaction: An experimental study on ultrapotassic rocks from Alban Hills (Central Italy). *Lithos*, *101*(3–4), 397–415. https://doi.org/10.1016/j.lithos.2007.08.008

Friedman, J. H. (2002). Stochastic gradient boosting. *Computational Statistics and Data Analysis*, *38*(4), 367–378. https://doi.org/10.1016/S0167-9473(01)00065-2

Fujii, T., & Bougault, H. (1983). Melting relations of a magnesian abyssal tholeiite and the origin of MORBs. *Earth and Planetary Science Letters*, *62*(2), 283–295. https://doi.org/10.1016/0012-821X(83)90091-2

Gaetani, G. A., & Grove, T. L. (1998). The influence of water on melting of mantle peridotite. *Contributions to Mineralogy and Petrology*, *131*(4), 323–346. https://doi.org/10.1007/s004100050396

Gaetani, G. A. (2004). The influence of melt structure on trace element partitioning near the

peridotite solidus. *Contributions to Mineralogy and Petrology*, *147*, 511–527. https://doi.org/10.1007/s00410-004-0575-1

Gee, L. L., & Sack, R. O. (1988). Experimental petrology of melilite nephelinites. *Journal of Petrology*, *29*(6), 1233–1255. https://doi.org/10.1093/petrology/29.6.1233

Geiger, H., Mattsson, T., Deegan, F. M., Troll, V. R., Burchardt, S., Gudmundsson, Ó., et al. (2016). Magma plumbing for the 2014-2015 Holuhraun eruption, Iceland. *Geochemistry Geophysics Geosystems*, *17*(8), 2953–2968

Geurts, P., Ernst, D., & Wehenkel, L. (2006). Extremely randomized trees. *Machine Learning*, *63*(1), 3–42. https://doi.org/10.1007/s10994-006-6226-1

Grove, T. L., & Bryan, W. B. (1983). Fractionation of pyroxene-phyric MORB at low pressure: An experimental study. *Contributions to Mineralogy and Petrology*, *84*(4), 293–309. https://doi.org/10.1007/BF01160283

Grove, T. L., & Juster, T. C. (1989). Experimental investigations of low-Ca pyroxene stability and olivine-pyroxene-liquid equilibria at 1-atm in natural basaltic and andesitic liquids. *Contributions to Mineralogy and Petrology*, *103*(3), 287–305. https://doi.org/10.1007/BF00402916

Grove, T. L., Gerlach, D. C., & Sando, T. W. (1982). Origin of calc-alkaline series lavas at Medicine Lake Volcano by fractionation, assimilation and mixing. *Contributions to Mineralogy and Petrology*, *80*(2), 160–182. https://doi.org/10.1007/BF00374893

Grove, T. L., Kinzler, R. J., & Bryan, W. B. (1992). Fractionation of Mid-Ocean Ridge Basalt (MORB). In *Mantle Flow and Melt Generation at Mid-Ocean Ridges* (pp. 281–310). American Geophysical Union (AGU). https://doi.org/10.1029/GM071p0281

Grove, T. L., Donnelly-Nolan, J. M., & Housh, T. (1997). Magmatic processes that generated the rhyolite of Glass Mountain, Medicine Lake volcano, N. California. *Contributions to Mineralogy and Petrology*, *127*(3), 205–223. https://doi.org/10.1007/s004100050276

Grove, T. L., Elkins-Tanton, L. T., Parman, S. W., Chatterjee, N., Müntener, O., & Gaetani, G. A. (2003). Fractional crystallization and mantle-melting controls on calc-alkaline differentiation trends. *Contributions to Mineralogy and Petrology*, *145*(5). https://doi.org/10.1007/s00410-003-0448-z

Halldórsson, S. A., Bali, E., Hartley, M. E., Neave, D. A., Peate, D. W., Guðfinnsson, G. H., et al. (2018). Petrology and geochemistry of the 2014–2015 Holuhraun eruption, central Iceland: compositional and mineralogical characteristics, temporal variability and magma storage. *Contributions to Mineralogy and Petrology*, *173*(8). https://doi.org/10.1007/s00410-018-1487-9

Hartley, M. E., Bali, E. o, Maclennan, J., Neave, D. A., & Halldórsson, S. A. (2018). Melt inclusion constraints on petrogenesis of the 2014-2015 Holuhraun eruption, Iceland. *Contribution to Mineralogy and Petrology*, *173*(2).

Hartley, M. E., & Thordarson, T. (2013). The 1874-1876 volcano-tectonic episode at Askja, North Iceland: Lateral flow revisited. *Geochemistry, Geophysics, Geosystems*, *14*(7), 2286–2309. https://doi.org/10.1002/ggge.20151

Hazen, R. M. (2014). Data-driven abductive discovery in mineralogy. *American Mineralogist*, *99*(11–12), 2165–2170. https://doi.org/10.2138/am-2014-4895

Hazen, R. M., Downs, R. T., Eleish, A., Fox, P., Gagné, O. C., Golden, J. J., et al. (2019). Data-Driven Discovery in Mineralogy: Recent Advances in Data Resources, Analysis, and Visualization. *Engineering*, *5*(3), 397–405. https://doi.org/10.1016/j.eng.2019.03.006

Helz, R. T., & Thornber, C. R. (1987). Geothermometry of Kilauea Iki lava lake, Hawaii. *Bulletin of Volcanology*, *49*(5), 651–668. https://doi.org/10.1007/BF01080357

Hesse, M., & Grove, T. L. (2003). Absarokites from the western Mexican Volcanic Belt: Constraints on mantle wedge conditions. *Contributions to Mineralogy and Petrology*, *146*(1), 10–27. https://doi.org/10.1007/s00410-003-0489-3

Hirschmann, M. M., Kogiso, T., Baker, M. B., & Stolper, E. M. (2003). Alkalic magmas generated by partial melting of garnet pyroxenite. *Geology*, *31*(6), 481–484. https://doi.org/10.1130/0091-7613(2003)031<0481:AMGBPM>2.0.CO;2

Hirschmann, M. M., Ghiorso, M. S., Davis, F. A., Gordon, S. M., Mukherjee, S., Grove, T. L., et al. (2008). Library of Experimental Phase Relations (LEPR): A database and Web portal for experimental magmatic phase equilibria data. *Geochemistry, Geophysics, Geosystems*, *9*(3). https://doi.org/10.1029/2007GC001894

Ho, T. K. (1998). The random subspace method for constructing decision forests. IEEE Transactions on Pattern Analysis and Machine Intelligence, 20(8), 832–844. https://doi.org/10.1109/34.709601

Holbig, E. S., & Grove, T. L. (2008). Mantle melting beneath the Tibetan Plateau: Experimental constraints on ultrapotassic magmatism. *Journal of Geophysical Research: Solid Earth*, *113*(4). https://doi.org/10.1029/2007JB005149

Johnson, K. T. M. (1998). Experimental determination of partition coefficients for rare earth and high-field-strength elements between clinopyroxene, garnet, and basaltic melt at high pressures. *Contributions to Mineralogy and Petrology*, *133*(1–2), 60–68. https://doi.org/10.1007/s004100050437

Johnston, A. D. (1986). Anhydrous P-T phase relations of near-primary high-alumina basalt

from the South Sandwich Islands - Implications for the origin of island arcs and tonalite-trondhjemite series rocks. *Contributions to Mineralogy and Petrology*, *92*(3), 368–382. https://doi.org/10.1007/BF00572166

Juster, T. C., Grove, T. L., & Perfit, M. R. (1989). Experimental constraints on the generation of FeTi basalts, andesites, and rhyodacites at the Galapagos Spreading Center, 85°W and 95°W. *Journal of Geophysical Research*, *94*(B7), 9251–9274. https://doi.org/10.1029/JB094iB07p09251

Kägi, R., Müntener, O., Ulmer, P., & Ottolini, L. (2005). Piston-cylinder experiments on H_2O undersaturated Fe-bearing systems: An experimental setup approaching f_{O2} conditions of natural calc-alkaline magmas. *American Mineralogist*, *90*(4), 708–717. https://doi.org/10.2138/am.2005.1663

Kawamoto, T. (1996). Experimental constraints on differentiation and H_2O abundance of calc-alkaline magmas. *Earth and Planetary Science Letters*, *144*(3–4), 577–589.

Kelemen, P. B., Joyce, D. B., Webster, J. D., & Holloway, J. R. (1990). Reaction between ultramafic rock and fractionating basaltic magma II. experimental investigation of reaction between olivine tholeiite and harzburgite at 1150-1050°C and 5 kb. *Journal of Petrology*, *31*(1), 99–134. https://doi.org/10.1093/petrology/31.1.99

Kennedy, A. K., Grove, T. L., & Johnson, R. W. (1990). Experimental and major element constraints on the evolution of lavas from Lihir Island, Papua New Guinea. *Contributions to Mineralogy and Petrology*, *104*(6), 722–734. https://doi.org/10.1007/BF01167289

Kennedy, B. M., Holohan, E. P., Stix, J., Gravley, D. M., Davidson, J. R. J., & Cole, J. W. (2018). Magma plumbing beneath collapse caldera volcanic systems. *Earth-Science Reviews*, *177*, 404–424. https://doi.org/10.1016/J.EARSCIREV.2017.12.002

Keshav, S., Gudfinnsson, G. H., Sen, G., & Fei, Y. (2004). High-pressure melting experiments on garnet clinopyroxenite and the alkalic to tholeiitic transition in ocean-island basalts. *Earth and Planetary Science Letters*, *223*(3–4), 365–379. https://doi.org/10.1016/j.epsl.2004.04.029

Kinzler, R. J. (1997). Melting of mantle peridotite at pressures approaching the spinel to garnet transition: Application to mid-ocean ridge basalt petrogenesis. *Journal of Geophysical Research B: Solid Earth*, *102*(B1), 853–874.

Kinzler, R. J., & Grove, T. L. (1985). Crystallization and differentiation of Archean komatiite lavas from northeast Ontario: phase equilibrium and kinetic studies. *American Mineralogist*, *70*(1–2), 40–51.

Kinzler, R. J., & Grove, T. L. (1992). Primary magmas of mid-ocean ridge basalts 1. Experiments and methods. *Journal of Geophysical Research*, *97*(B5), 6885–6906. https://doi.org/10.1029/91JB02840

Kjarsgaard, B. A. (1998). Phase relations of a carbonated high-CaO nephelinite at 0.2 and 0.5 GPa. *Journal of Petrology*, *39*(11–12), 2061–2075. https://doi.org/10.1093/petroj/39.11-12.2061

Koester, E., Pawley, A. R., Fernandes, L. A. D., Porcher, C. C., & Soliani Jr., E. (2002). Experimental melting of cordierite gneiss and the petrogenesis of syntranscurrent peraluminous granites in Southern Brazil. *Journal of Petrology*, *43*(8), 1595–1616.

Kogiso, T., & Hirschmann, M. M. (2001). Experimental study of clinopyroxenite partial melting and the origin of ultra-calcic melt inclusions. *Contributions to Mineralogy and Petrology*, *142*(3), 347–360. https://doi.org/10.1007/s004100100295

Kogiso, T., Hirose, K., & Takahashi, E. (1998). Melting experiments on homogeneous mixtures of peridotite and basalt: Application to the genesis of ocean island basalts. *Earth and Planetary Science Letters*, *162*(1–4), 45–61. https://doi.org/10.1016/S0012-821X(98)00156-3

Ishii, T., Robinson, P.T., Maekawa, H., Fiske, R. (1992). Petrological studies of peridotites from diapiric serpentinite seamounts in the Izu-Ogasawara-Mariana Forearc, Leg 125. *Proc. Ocean Drill. Program, Sci. Results* 125, 445–486. https://doi.org/10.2973/odp.proc.sr.125.129.1992

Itano, K., Ueki, K., Iizuka, T., & Kuwatani, T. (2020). Geochemical discrimination of monazite source rock based on machine learning techniques and multinomial logistic regression analysis. *Geosciences*, *10*(2). https://doi.org/10.3390/geosciences10020063

Laporte, D., Toplis, M. J., Seyler, M., & Devidal, J.-L. (2004). A new experimental technique for extracting liquids from peridotite at very low degrees of melting: Application to partial melting of depleted peridotite. *Contributions to Mineralogy and Petrology*, *146*(4), 463–484. https://doi.org/10.1007/s00410-003-0509-3

Li, X., Zhang, C., Behrens, H., & Holtz, F. (2020). Calculating amphibole formula from electron microprobe analysis data using a machine learning method based on principal components regression. *Lithos*, *362–363*. https://doi.org/10.1016/j.lithos.2020.105469

Louppe, G., Wehenkel, L., Sutera, A., & Geurts, P. (2013). Understanding variable importances in Forests of randomized trees. In: Burges, C., J., C., Bottou, L., Welling, M., Ghahramani, Z., Weinberger K., Q., (Eds.), Adv. Neural Inf. Process. Syst. 26, Curran Associates, Inc., 2013, pp.431–439

Masotta, M., Mollo, S., Freda, C., Gaeta, M., & Moore, G. (2013). Clinopyroxene–liquid thermometers and barometers specific to alkaline differentiated magmas. *Contributions to Mineralogy and Petrology*, *166*(6), 1545–1561. https://doi.org/10.1007/s00410-013-0927-9

Mollo, S., Putirka, K., Misiti, V., Soligo, M., & Scarlato, P. (2013). A new test for equilibrium based on clinopyroxene-melt pairs: Clues on the solidification temperatures of Etnean alkaline melts at post-eruptive conditions. *Chemical Geology*, *352*, 92–100. https://doi.org/10.1016/j.chemgeo.2013.05.026

Mollo, S., Blundy, J., Scarlato, P., De Cristofaro, S. P., Tecchiato, V., Di Stefano, F., et al. (2018). An integrated P-T-H_2O-lattice strain model to quantify the role of clinopyroxene fractionation on REE+Y and HFSE patterns of mafic alkaline magmas: Application to eruptions at Mt. Etna. *Earth-Science Reviews*, *185*, 32–56. https://doi.org/10.1016/j.earscirev.2018.05.014

Montgomery, D., C. Peck, E. A., & Vining, G. G. (2012). *Introduction to linear regression analysis* (5th ed.). John Wiley & Sons, Inc. ISBN: 978-0-470-54281-1

Montierth, C., Johnston, A. D., & Cashman, K. V. (1995). *An empirical glass-composition-based geothermometer for Mauna Loa Lavas*. *Geophysical Monograph Series* (Vol. 92). https://doi.org/10.1029/GM092p0207

Morrison, S. M., Liu, C., Eleish, A., Prabhu, A., Li, C., Ralph, J., et al. (2017). Network analysis of mineralogical systems. *American Mineralogist*, *102*(8), 1588–1596. https://doi.org/10.2138/am-2017-6104CCBYNCND

Nandedkar, R. H., Ulmer, P., & Müntener, O. (2014). Fractional crystallization of primitive, hydrous arc magmas: An experimental study at 0.7 GPa. *Contributions to Mineralogy and Petrology*, *167*(6), 1–27. https://doi.org/10.1007/s00410-014-1015-5

Natekin, A., & Knoll, A. (2013). Gradient boosting machines, a tutorial. Frontiers in Neurorobotics, 7(DEC). https://doi.org/10.3389/fnbot.2013.00021

Neave, D.A., Maclennan, J., Thordarson, T., Hartley, M.E. (2015). The evolution and storage of primitive melts in the Eastern Volcanic Zone of Iceland: the 10 ka Grímsvötn tephra series (i.e. the Saksunarvatn ash). *Contributions to Mineralogy and Petrology*

170,21. https://doi.org/10.1007/s00410-015-1170-3

Neave, D. A., & Putirka, K. D. (2017). A new clinopyroxene-liquid barometer, and implications for magma storage pressures under Icelandic rift zones. *American Mineralogist*, *102*(4), 777–794. https://doi.org/10.2138/am-2017-5968

Neave, D. A., Bali, E., Guðfinnsson, G. H., Halldórsson, A., Kahl, M., Schmidt, A., & Holtz,

F. (2019). Clinopyroxene–liquid equilibria and geothermobarometry in natural and experimental tholeiites: the 2014–2015 Holuhraun eruption, Iceland David. *Journal of Petrology*, 60 (8), 1653–1680. https://doi.org/10.1093/petrology/egz042

Nimis, P. (1995). A Clinopyroxene Geobarometer for Basaltic Systems Based on Crystal-Structure Modeling. *Contribution to Mineralogy and Petrology*, *121*(2), 115–125.

Nimis, P., & Ulmer, P. (1998). Clinopyroxene geobarometry of magmatic rocks Part 1: An expanded structural geobarometer for anhydrous and hydrous, basic and ultrabasic systems. *Contribution to Mineralogy and Petrology*, *133*(1–2), 122–135.

Pedregosa, F., Varoquaux, G. G., Gramfort, A., Michel, V., Thirion, B., Grisel, O., et al. (2011). Scikit-learn: Machine Learning in Python. *Journal of Machine Learning Research*, *12*, 2825–2830.

Petrelli, M., & Perugini, D. (2016). Solving petrological problems through machine learning: the study case of tectonic discrimination using geochemical and isotopic data. *Contributions to Mineralogy and Petrology*, *171*(10). https://doi.org/10.1007/s00410-016-1292-2

Petrelli, M., Bizzarri, R., Morgavi, D., Baldanza, A., & Perugini, D. (2017). Combining machine learning techniques, microanalyses and large geochemical datasets for tephrochronological studies in complex volcanic areas: New age constraints for the Pleistocene magmatism of central Italy. *Quaternary Geochronology*, *40*(2017), 33–44. https://doi.org/10.1016/j.quageo.2016.12.003

Petrelli, M., El Omari, K., Spina, L., Le Guer, Y., La Spina, G., & Perugini, D. (2018). Timescales of water accumulation in magmas and implications for short warning times of explosive eruptions. *Nature Communications*, *9*(1), 770. https://doi.org/10.1038/s41467-018-02987-6

Petrone, C. M., Bugatti, G., Braschi, E., & Tommasini, S. (2016). Pre-eruptive magmatic processes re-timed using a non-isothermal approach to magma chamber dynamics. *Nature Communications*, *7*. https://doi.org/10.1038/ncomms12946

Petrone, C. M., Braschi, E., Francalanci, L., Casalini, M., & Tommasini, S. (2018). Rapid mixing and short storage timescale in the magma dynamics of a steady-state volcano. *Earth and Planetary Science Letters*, *492*, 206–221. https://doi.org/10.1016/j.epsl.2018.03.055

Putirka, K. D. (1999). Clinopyroxene + liquid equilibria to 100 kbar and 2450 K. *Contributions to Mineralogy and Petrology*, *135*(2–3), 151–163. https://doi.org/10.1007/s004100050503

Putirka, K. D. (2018). *Geothermometry and geobarometry*. *Encyclopedia of Earth Sciences*

Series. https://doi.org/10.1007/978-3-319-39312-4_322

Putirka, K. D. Thermometers and barometers for volcanic systems, 69 Minerals, Inclusions and Volcanic Processes § (2008). https://doi.org/10.2138/rmg.2008.69.3

Putirka, K. D., Mikaelian, H., Ryerson, F., & Shaw, H. (2003). New clinopyroxene-liquid thermobarometers for mafic, evolved, and volatile-bearing lava compositions, with applications to lavas from Tibet and the Snake River Plain, Idaho. *American Mineralogist*, *88*(10), 1542–1554. https://doi.org/10.2138/am-2003-1017

Ren, Q., Li, M., Han, S., Zhang, Y., Zhang, Q., & Shi, J. (2019). Basalt tectonic discrimination using combined machine learning approach. *Minerals*, *9*(6). https://doi.org/10.3390/min9060376

Shai, S.-S., & Shai, B.-D. (2014). *Understanding Machine Learning: From Theory to Algorithms*. Cambridge University Press. ISBN: 978-1107057135

Tarasewicz, J., White, R. S., Woods, A. W., Brandsdóttir, B., & Gudmundsson, M. T. (2012). Magma mobilization by downward-propagating decompression of the Eyjafjallajkull volcanic plumbing system. *Geophysical Research Letters*, *39*(19). https://doi.org/10.1029/2012GL053518

Thornber, C. R., Heliker, C., Sherrod, D. R., Kauahikaua, J. P., Miklius, A., Okubo, P. G., et al. (2003). Kilauea east rift zone magmatism: An episode 54 perspective. *Journal of Petrology*, *44*(9), 1525–1559.

Ubide, T., & Kamber, B. S. (2018). Volcanic crystals as time capsules of eruption history. *Nature Communications*, *9*(1), 326. https://doi.org/10.1038/s41467-017-02274-w

Ueki, K., Kuwatani, T., Okamoto, A., Akaho, S., & Iwamori, H. (2020). Thermodynamic modeling of hydrous-melt–olivine equilibrium using exhaustive variable selection. *Physics of the Earth and Planetary Interiors*, *300*, 106430. https://doi.org/10.1016/j.pepi.2020.106430

Vander Auwera, J., & Longhi, J. (1994). Experimental study of a jotunite (hypersthene monzodiorite): constraints on the parent magma composition and crystallization conditions (P, T, f_{O2}) of the Bjerkreim-Sokndal layered intrusion (Norway). *Contributions to Mineralogy and Petrology*, *118*(1), 60–78. https://doi.org/10.1007/BF00310611

Vander Auwera, J., Longhi, J., & Dughesne, J.-G. (1998). A liquid line of descent of the jotunite (hypersthene monzodiorite) suite. *Journal of Petrology*, *39*(3), 439–468. https://doi.org/10.1093/petroj/39.3.439

Villiger, S., Ulmer, P., Müntener, O., & Thompson, A. B. (2004). The liquid line of descent of

anhydrous, mantle-derived, tholeiitic liquids by fractional and equilibrium crystallization - An experimental study at 1·0 GPa. *Journal of Petrology*, *45*(12), 2369–2388. https://doi.org/10.1093/petrology/egh042

Villiger, S., Ulmer, P., & Müntener, O. (2007). Equilibrium and fractional crystallization experiments at 0.7 GPa; the effect of pressure on phase relations and liquid compositions of tholeiitic magmas. *Journal of Petrology*, *48*(1), 159–184. https://doi.org/10.1093/petrology/egl058

Winpenny, B., & Maclennan, J. (2011). A partial record of mixing of mantle melts preserved in icelandic phenocrysts. *Journal of Petrology*, *52*(9), 1791–1812. https://doi.org/10.1093/petrology/egr031

Yang, H.-J., Kinzler, R. J., & Grove, T. L. (1996). Experiments and models of anhydrous, basaltic olivine-plagioclase-augite saturated melts from 0.001 to 10 kbar. *Contributions to Mineralogy and Petrology*, *124*(1), 1–18. https://doi.org/10.1007/s004100050169

Zhang, Y., & Haghani, A. (2015). A gradient boosting method to improve travel time prediction. Transportation Research Part C: Emerging Technologies, 58, 308–324. https://doi.org/10.1016/j.trc.2015.02.019

Zellmer, G. F., Sakamoto, N., Iizuka, Y., Miyoshi, M., Tamura, Y., Hsieh, H.-H., & Yurimoto, H. (2014). *Crystal uptake into aphyric arc melts: Insights from two-pyroxene pseudo-decompression paths, plagioclase hygrometry, and measurement of hydrogen in olivines from mafic volcanics of SW Japan*. *Geological Society Special Publication* (Vol. 385). https://doi.org/10.1144/SP385.3

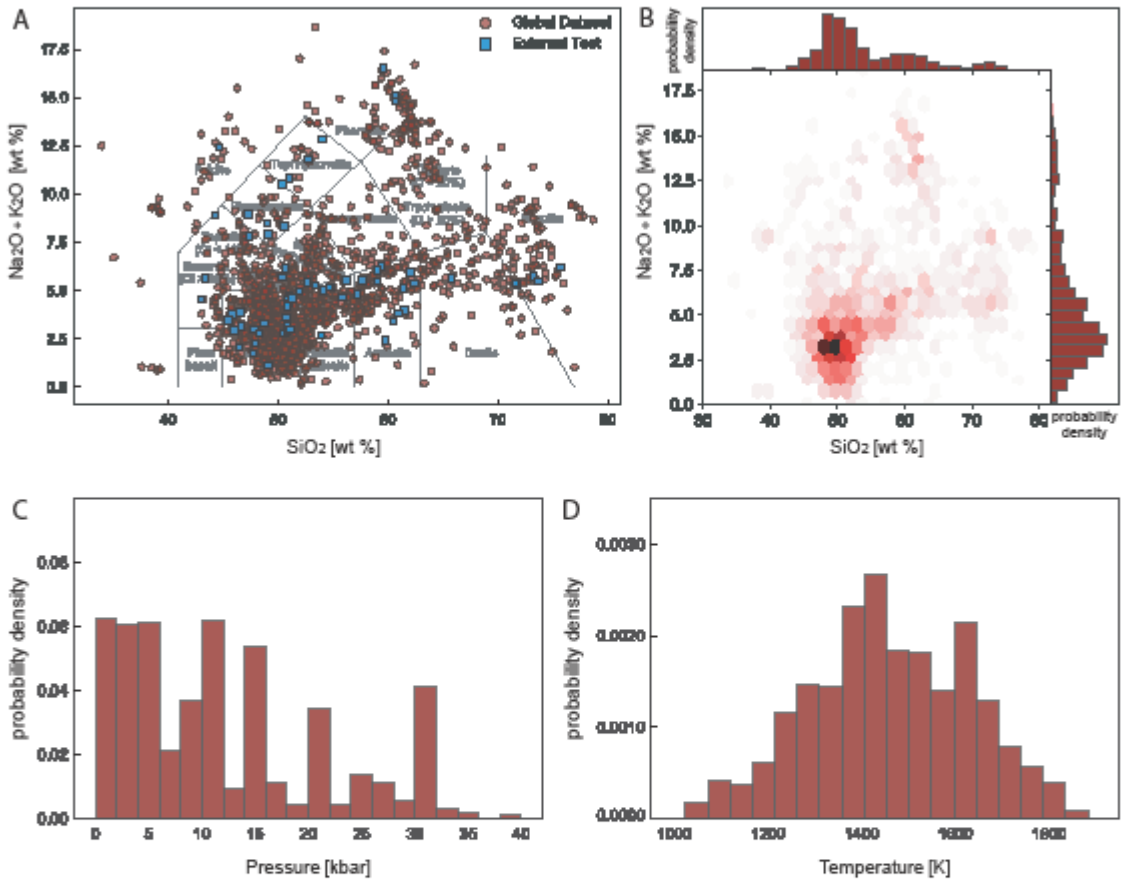

Figure 1. Total Alkaly vs. Silica diagram (A) and probability density distributions for SiO_2 and $Na_2O + K_2O$ (B) of the global dataset utilized in the present study. A) Total Alkaly vs. Silica diagram dyspling the train-test (in red) and the external check (in blue) dataset, respectively. B) Probability density distribution for SiO_2 and $Na_2O + K_2O$.

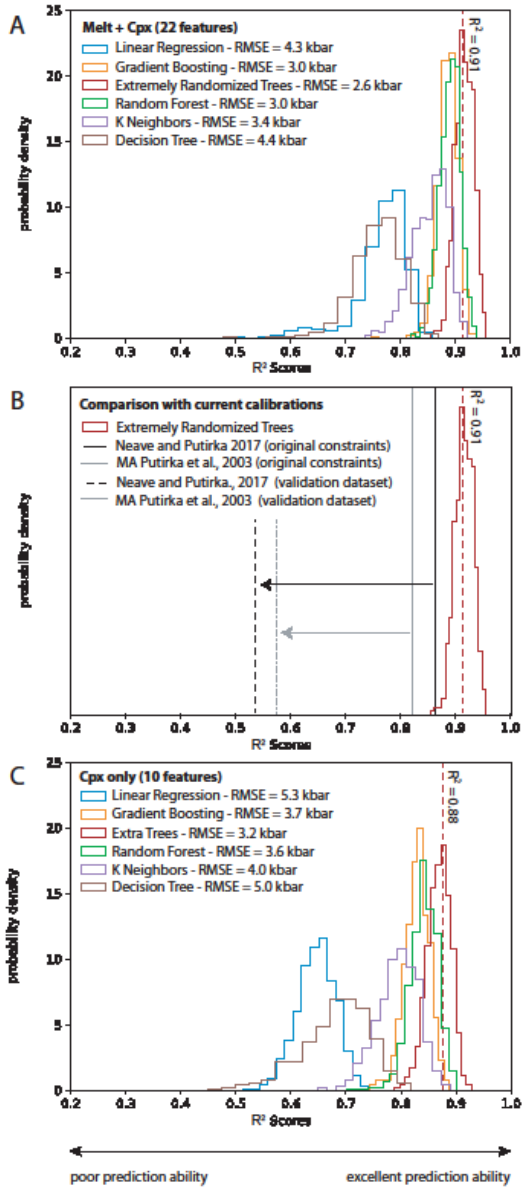

Figure 2. Probability density distributions of the coefficient of determination (R^2) for pressure estimations on the validation datasets: A) Comparison among the Machine learning algorithms calibrated using clinopyroxene-liquid pairs (22 features); A) Comparison between the Extremely Randomized Trees regression ML algorithm and regression based thermodynamic models currently available in literature, all calibrated using clinopyroxene-liquid pairs (22 features); C) Comparison among the Machine learning algorithms calibrated using clinopyroxene analyses only (10 features).

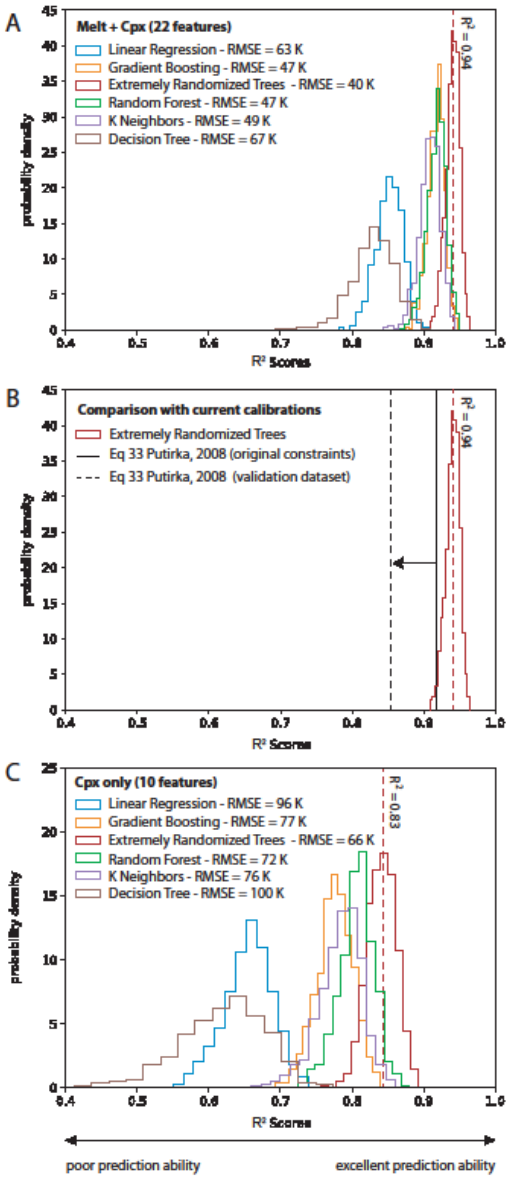

Figure 3. Probability density distributions of the coefficient of determination (R^2) for temperature estimations on the validation datasets: A) Comparison among the Machine learning algorithms calibrated using clinopyroxene-liquid pairs (22 features); A) Comparison between the Extremely Randomized Trees regression ML algorithm and regression based thermodynamic models currently available in literature, all calibrated using clinopyroxene-liquid pairs (22 features); C) Comparison among the Machine learning algorithms calibrated using clinopyroxene analyses only (10 features).

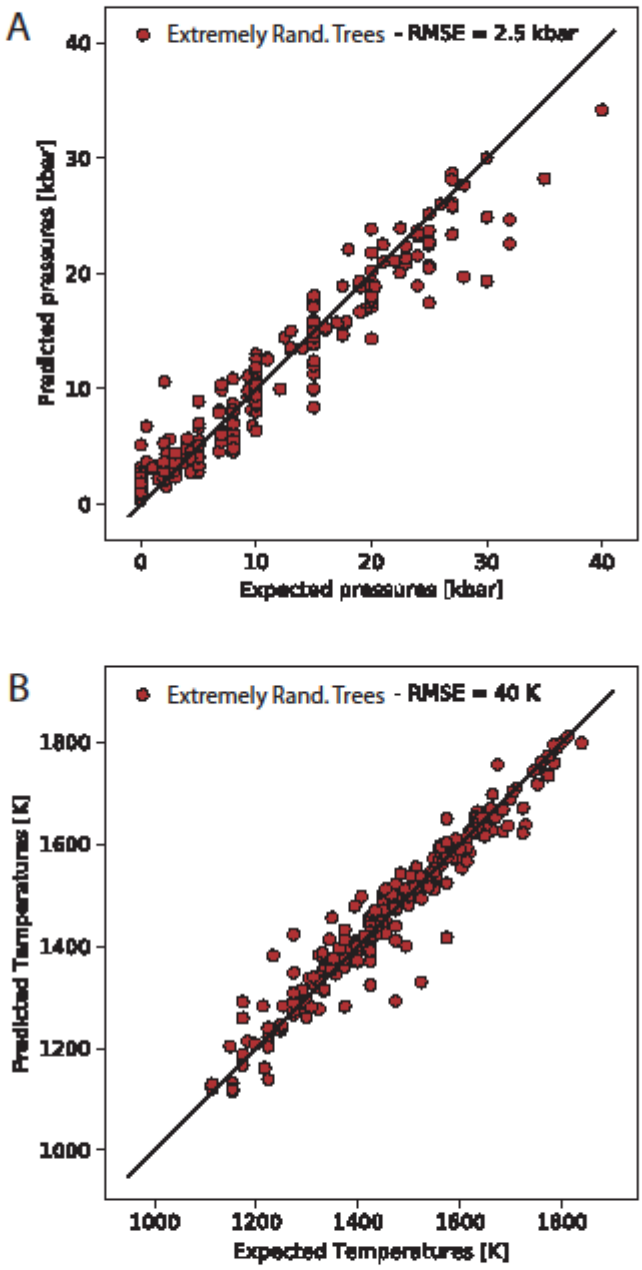

Figure 4. Binary plot reporting the figures of merits (R^2 and RMSE) for the pressure (A) and temperature (B) estimations performed during one of the 1000 repetitions of the random splitting of the dataset, training and subsequent test. RMSE are 2.5 kbar and 40 K, for the pressure and temperature, respectively.

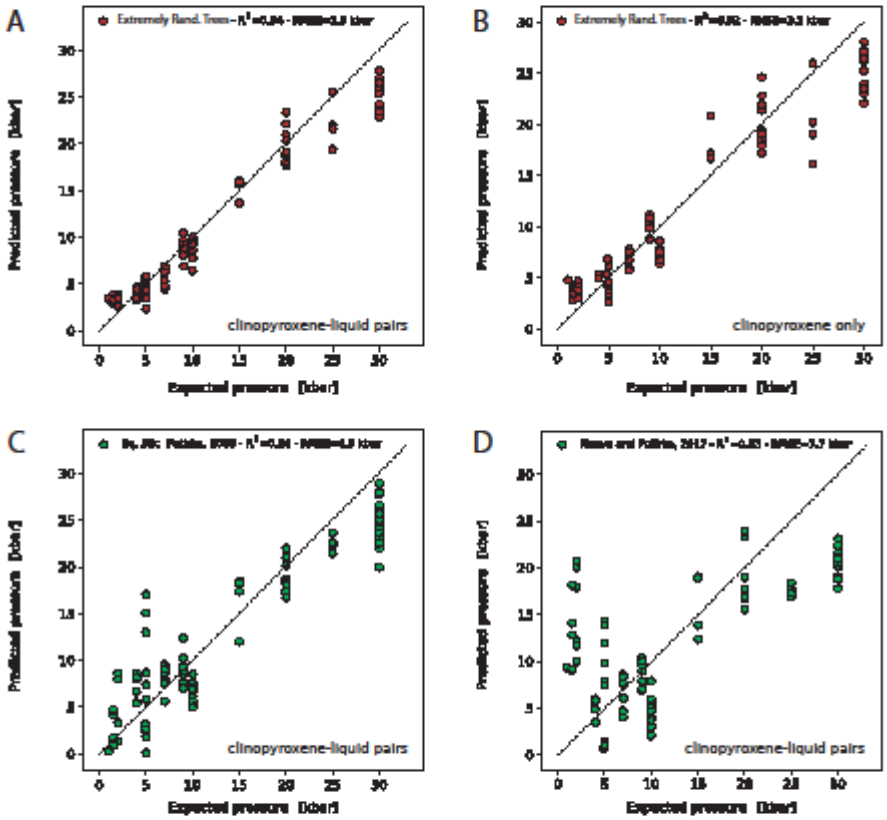

Figure 5. Binary plot reporting the figures of merits (R^2 and RMSE) for pressure estimations performed on the test dataset. A) Extremely Randomized Trees regression on clinopyroxene-liquid pairs (i.e., 22 features); B) Extremely Randomized Trees regression on clinopyroxene analyses (i.e., 10 features); C) Equation 32c (Putirka, 2008) on clinopyroxene-liquid pairs; C) Model A (Putirka et al., 2003) on clinopyroxene-liquid pairs.

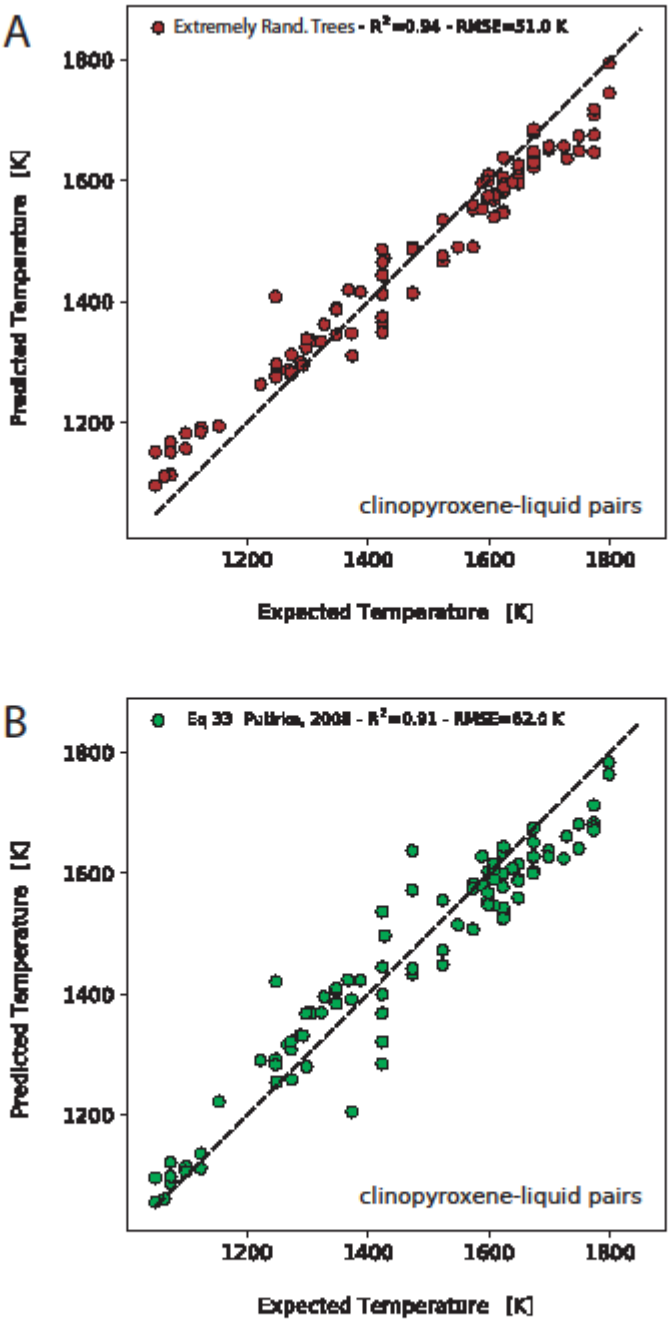

Figure 6. Binary plot reporting the figures of merits (R^2 and RMSE) for temperature estimations performed on the test dataset. A) Extremely Randomized Trees regression on clinopyroxene-liquid pairs (i.e., 22 features); B) Eq. 33 (Putirka, 2008) on clinopyroxene-liquid pairs.of the Extremely Randomized Trees regression algorithm: A) training for pressure estimations; b) training for temperature estimations. The R^2 of both cpx-melt and cpx-only calibrations are also reported.

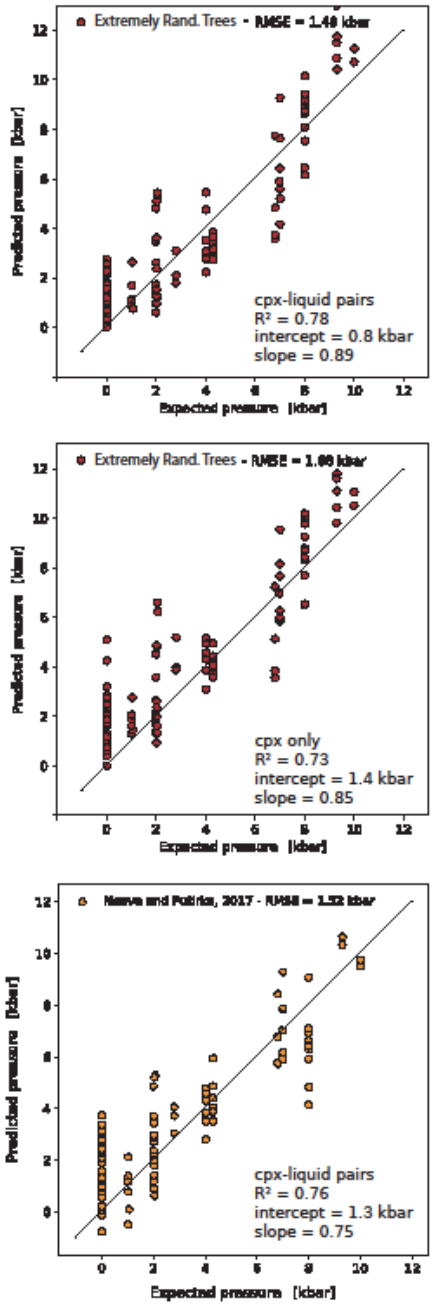

Figure 8. Binary plot reporting the figures of merits (R^2, RMSE, and regression statistics) for pressure estimations performed on the Tholeiites dataset check reported in Neave and Putirka (2017). A) Extremely Randomized Trees regression on clinopyroxene-liquid pairs (i.e., 22 features); B) Extremely Randomized Trees regression on clinopyroxene analyses (i.e., 10 features); C) Caribration for P reported by Neave and Putirka (2017) on clinopyroxene-liquid pairs.

reported by Neave and Putirka (2017) (in blue). B) Probability density distribution and kernel density estimations for pressure estimations of the liquid-clinopyroxene pairs generated by marching the analysis '292' with all the magmas that are in apparent equilibrium with it.

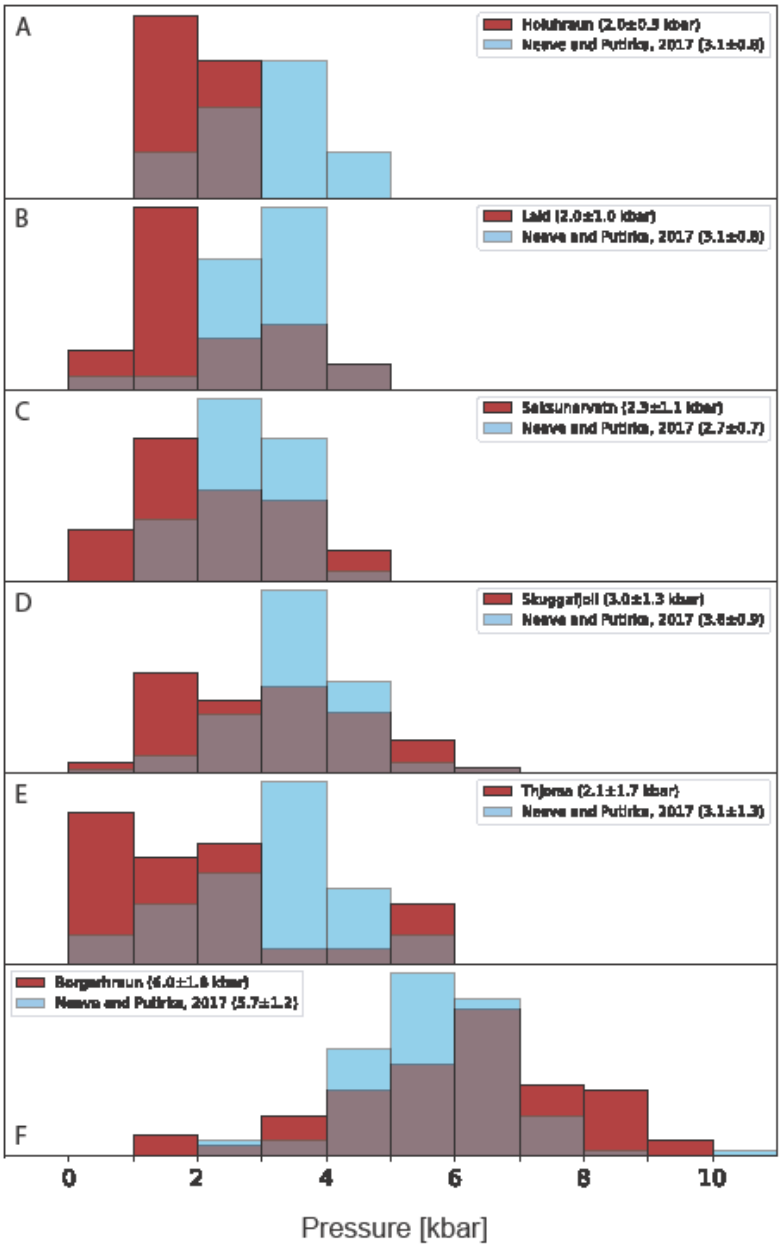

Figure 10. Probability density distributions for crystallization pressures obtained by the application of the fully clinopyroxene based ML calibration on the analyses reported by Neave and Putirka (2017). A) Holuhran; B) Laki; C) Saksunarvatn; D) Skuggafjoll; E)Thjorsa; F) Borgarhraun. Results reported by Neave and Putirka (2017) are also reported as reference.

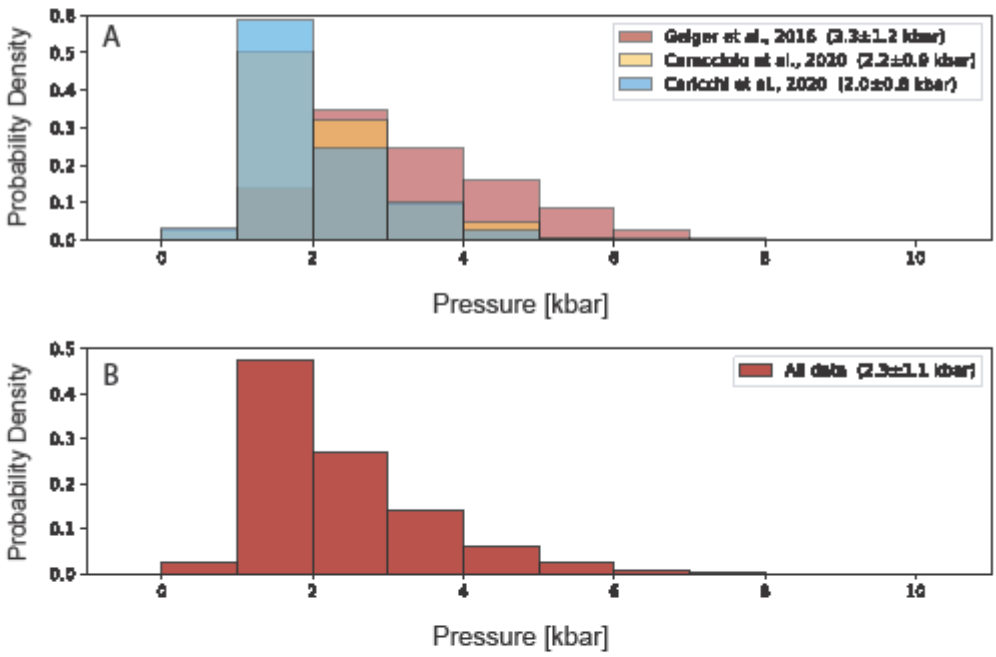

Figure 11. Probability density distributions for crystallization pressures obtained by the application of the fully clinopyroxene based ML calibration on the Barðarbunga volcanic system: A) data by Caracciolo et al. (2020) for eruptions in the time range of 100 ka to 1477AD, Caricchi et al. (2020) and Geiger et al. (2016) for the 2014-15 Holuhraun eruption; B) A combination of pressure estimates in panel A.

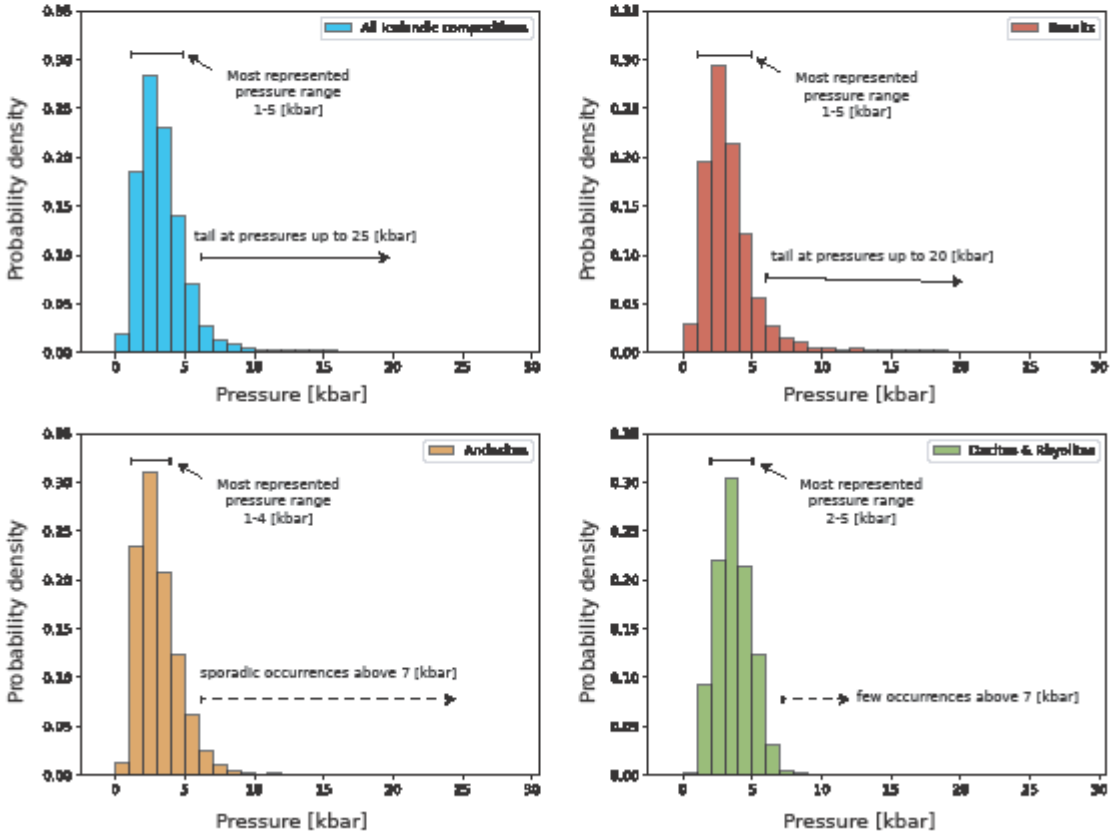

Figure 12. Probability density distributions for crystallization pressures obtained by the application of the fully clinopyroxene based ML calibration on cpx analyses from Georoc: A) the whole dataset; B) cpx hosted in basaltic magmas; C) cpx hosted in andesitic magmas; B) cpx hosted in dacitic and rhyolitic magmas.

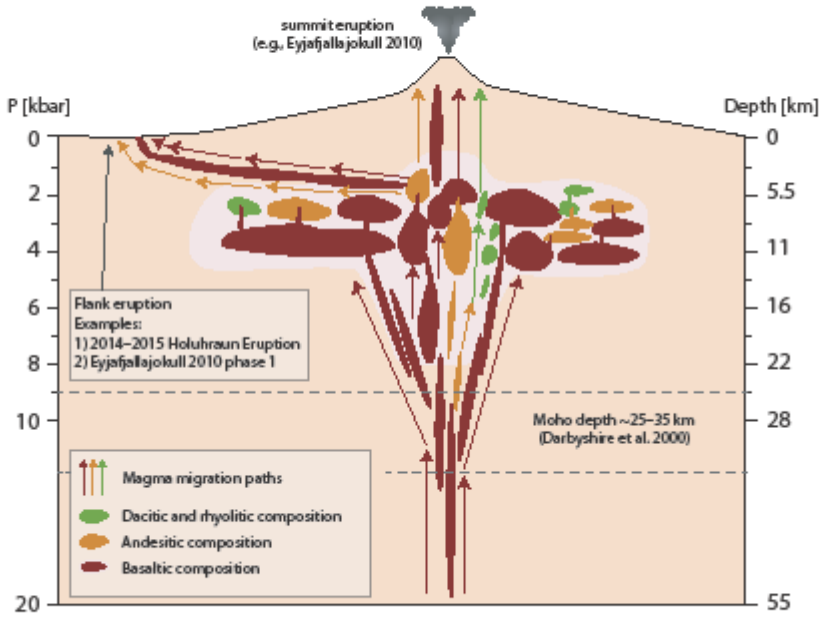

Figure 13. Schematic view of a generalized volcanic plumbing system below Icelandic volcanoes based on the results reported in the present manuscript. Examples of recent eruption are also reported.